Determining the Surfactant Consistent with Concrete in order to Achieve the Maximum Possible Dispersion of Multiwalled Carbon Nanotubes in Keeping the Plain Concrete

Numerical Methods for the Solution of Population Balance Equations Coupled with Computational Fluid Dynamics

Mohsen Shiea, Antonio Buffo, Marco Vanni, and Daniele Marchisio

Department of Applied Science and Technology, Institute of Chemical Engineering, Politecnico di Torino, Torino, Italy; corresponding author: Daniele Marchisio; e-mail: daniele.marchisio@polito.it

Xxxx. Xxx. Xxx. Xxx. YYYY. AA:1–24

https://doi.org/10.1146/((please add article doi))

Keywords

population balance equation, computational fluid dynamics, multiphase flow, crystallization, gas-liquid systems, liquid-liquid systems, quadrature-based moment methods

Abstract

This review article discusses the solution of population balance equations, for the simulation of disperse multiphase systems, tightly coupled with computational fluid dynamics. Although several methods are discussed, the focus is on quadrature-based moments methods (QBMM) with particular attention to the quadrature method of moments, the conditional quadrature method of moments and the direct quadrature method of moments. The relationship between the population balance equation, in its generalized form, and the Euler-Euler multiphase flow models, notably the two-fluid model, is thoroughly discussed. Then the closure problem and the use of Gaussian quadratures to overcome it is analyzed. The review concludes with the presentation of numerical issues and guidelines for users of these modelling approaches.

1. INTRODUCTION

Computational Fluid Dynamics (CFD) for simulation of disperse multiphase systems has gained considerable importance in the last two decades due to its widespread application in chemical, biochemical, pharmaceutical and aerospace industries. Disperse multiphase systems are formed by separate entities, i.e. particles/crystals, drops and bubbles, being dispersed in a continuous phase. The characteristic properties of the disperse phase elements change in space and time due to numerous particulate processes, such as collisions, aggregation/coalescence, breakage, nucleation, dissolution/evaporation, mass and heat transfer, etc. As a result, disperse systems often feature distributions of elements with different properties, a situation identified as polydispersity. A comprehensive simulation of disperse systems must take into account polydispersity and therefore must include the description of the above-mentioned processes. The most common computational approaches employed in this field can be categorized in three main groups: fully-resolved interface-tracking models, Lagrangian point-particle models and Eulerian-Eulerian models. This review focuses on the last group of methods, which has the simplest level of detail in comparison to the other two groups, however is suitable for CFD simulation of multiphase systems, particularly those of industrial-scale.

Eulerian-Eulerian methods in their original formulation (in the 90s) required the specification of the mean size of disperse phase elements. Being this number fixed and constant, it was simply impossible to account for polydispersity and for the effect of particulate processes. It was only in 00s that their coupling with Population Balance Equations (PBEs) was realized and the relationship between PBEs and Eulerian-Eulerian models was investigated and clarified. In this review, a critical discussion of these issues is reported. In particular, it will be explained how the solution of the PBE provides a detailed level of description of the disperse phase, which is not accessible from CFD models alone, leading to a more accurate simulation of the entire system. To this purpose, a suitable method for the solution of the PBE should be selected considering several factors such as the nature of the system under study, the required level of description and the available computational resources. The current review covers several methods for the solution of the PBE, which belong to three main categories: the class or sectional method, the method of moments and the quadrature-based moment method. Further, a separate section addresses the implementation of PBE in CFD and discusses some numerical issues concerning the stability of simulations. The review concludes by discussing the most popular implementations in commercial and open-source CFD-PBE codes.

2. GOVERNING EQUATIONS

2.1. Population Balance Equation

The PBE is a continuity statement that governs the evolution of a number density function (NDF), which is postulated to exist for a population of disperse phase elements. The NDF defines the distribution of the disperse phase elements over the properties of interest at any time instant and physical position. These properties, called internal coordinates, characterize the disperse elements and can include velocity, size, composition, temperature, etc. The choice of the internal coordinates, denoted here by the vector $\boldsymbol{\xi}$, is system dependent. The state of a generic element q at time t can be determined by its position vector $\mathbf{x}^{(q)}$ and internal coordinates $\boldsymbol{\xi}^{(q)}$, jointly called the element state vector $(\mathbf{x}^{(q)}, \boldsymbol{\xi}^{(q)})$. The state vector

of a given element specifies the location of that element in the so-called phase-space, which is a highly-dimensional space consisting of the physical domain of the system $\Omega_{\mathbf{x}}$ and the domain of the internal coordinates $\Omega_{\boldsymbol{\xi}}$. Given an arbitrary point in the phase-space $(\mathbf{x}, \boldsymbol{\xi})$, the NDF $n(t, \mathbf{x}, \boldsymbol{\xi})$ is defined as the expected number density of elements in the infinitesimal volume $\mathrm{d}\mathbf{x}\,\mathrm{d}\boldsymbol{\xi}$ around such point at time t (1).

At first, let the velocity of the disperse phase elements be known and excluded from the internal coordinate vector. Then the PBE takes the following form (2):

$$\partial_t n + \partial_{\mathbf{x}}(\mathbf{U}_{\mathrm{d}} n) + \partial_{\boldsymbol{\xi}}(\mathbf{G} n) = \mathcal{S}, \tag{1}$$

where $\mathbf{U}_{\mathrm{d}}(\boldsymbol{\xi})$ is the velocity of the disperse phase elements and $\mathbf{G}(\boldsymbol{\xi})$ the rate of change of the internal coordinates due to continuous molecular processes, such as mass and heat transfer, growth and dissolution of elements, chemical reactions etc. The source term $\mathcal{S}(\boldsymbol{\xi})$ describes the discontinuous changes in the internal coordinates of the elements due to discrete events, which are generally categorized as second-order, first-order and zero-order point processes. The mathematical form of $\mathcal{S}$ can be illustrated by the following example. If the only internal coordinate is the mass (or the volume) of the disperse phase elements which undergo aggregation/coalescence and breakage, then the source term becomes (space and time dependency is omitted for brevity) (1):

$$\mathcal{S}(\xi) = \frac{1}{2}\int_0^{\xi} a(\xi-\xi',\xi)\, n(\xi-\xi')\, n(\xi)\,\mathrm{d}\xi' - n(\xi)\int_0^{\infty} a(\xi,\xi')\, n(\xi')\,\mathrm{d}\xi' + \int_{\xi}^{\infty} b(\xi')\,\beta(\xi|\xi')\, n(\xi')\,\mathrm{d}\xi' - b(\xi)\, n(\xi), \tag{2}$$

where $a(\xi, \xi')$ denotes the rate of aggregation/coalescence between elements with internal coordinates equal to ξ and ξ' (i.e. aggregation kernel) and $b(\xi)$ the rate of breakage of elements with internal coordinate equal to ξ (i.e. breakage kernel). In addition, $\beta(\xi|\xi')$ is the so-called daughter distribution and statistically defines the number of daughter elements with internal coordinate equal to ξ formed due to the breakage of an element with internal coordinate of ξ'. In the RHS of Equation 2, the first and third terms describe the birth of new elements due to coalescence and breakage respectively, whereas the second and fourth terms take into account the death of elements due to coalescence and breakage respectively.

Equation 1 is a highly-dimensional transport (or kinetic) equation which describes the evolution of the NDF not only in time and physical space but also in the domain of internal coordinates. The velocity of the disperse phase in Equation 1 ($\mathbf{U}_{\mathrm{d}}$) is assumed to be a known function of time, spatial position and internal coordinates ($\boldsymbol{\xi}$). In addition, the flow fields of the continuous phase, e.g. velocity ($\mathbf{U}_{\mathrm{c}}$), are generally required by the closure relations for the description of both continuous and discontinuous processes, i.e. $\mathbf{G}$ and $\mathcal{S}$. For this purpose, the velocity of both phases ($\mathbf{U}_{\mathrm{d}}$ and $\mathbf{U}_{\mathrm{c}}$) can be obtained by adopting an Eulerian CFD approach, see Section 2.2.

The velocity of the disperse phase elements ($\mathbf{u}$) must be included within the internal coordinate vector when different elements (with or without the same properties) located at the same position $\mathbf{x}$ and at the time instant t move with different velocities. In this cases, the NDF $f(t, \mathbf{x}, \boldsymbol{\xi}, \mathbf{u})$ is defined as the expected number density of elements in the infinitesimal volume $\mathrm{d}\mathbf{x}\,\mathrm{d}\boldsymbol{\xi}\,\mathrm{d}\mathbf{u}$ around the arbitrary point $(\mathbf{x}, \boldsymbol{\xi}, \mathbf{u})$ at time t. The generalization of Equation 1 to include velocity as an internal coordinate leads to the following Generalized Population Balance Equation (GPBE) (2):

$$\partial_t f + \partial_{\mathbf{x}}(\mathbf{u} f) + \partial_{\boldsymbol{\xi}}(\mathbf{G} f) + \partial_{\mathbf{u}}(\mathbf{A} f) = \mathcal{S}. \tag{3}$$

Second-order point process: A discrete event that involves two disperse elements, such as collision and aggregation/coalescence

First-order point process: A discrete event that involves a single disperse element, such as breakage

Zero-order point process: A discrete event that does not involve any existing element, such as nucleation

Kinetic equation: NDF transport equation which includes the velocity of the elements as part of the internal coordinate vector

In Equation 3, $\mathbf{A}(\boldsymbol{\xi}, \mathbf{u})$ is the acceleration of the elements due to external forces, e.g. forces exerted from the continuous phase on the elements. The source term $\mathcal{S}(\boldsymbol{\xi}, \mathbf{u})$ is similar to that in the PBE except that it also describes the discontinuous change in the velocity of the elements due to discrete events (e.g. collisions).

It is noteworthy that Equation 3 is closely related to Equation 1. In fact, as highlighted in some specific applications (3–8), the GPBE can be simplified by presuming a specific form for the NDF, $f(t, \mathbf{x}, \boldsymbol{\xi}, \mathbf{u}) = n(t, \mathbf{x}, \boldsymbol{\xi})\, \delta(\mathbf{u} - \langle \mathbf{u}|\boldsymbol{\xi} \rangle)$, which is called the monokinetic assumption. This is equivalent to assuming that the elements with the same internal coordinates move with the same velocity (i.e. the mean velocity conditioned on the internal coordinates $\langle \mathbf{u}|\boldsymbol{\xi} \rangle$ (3)). Clearly this mean conditional velocity, defined as $\langle \mathbf{u}|\boldsymbol{\xi} \rangle = \int \mathbf{u} f \, \mathrm{d}\mathbf{u} \,/\, n(t, \mathbf{x}, \boldsymbol{\xi})$ is identical to $\mathbf{U}_\mathrm{d}(\boldsymbol{\xi})$, where $n(t, \mathbf{x}, \boldsymbol{\xi}) = \int f \, \mathrm{d}\mathbf{u}$ is the marginal NDF. The conditional velocity $\langle \mathbf{u}|\boldsymbol{\xi} \rangle$ can be calculated in different ways, by assuming for example a continuous parametric functional defined over the space of a chosen internal coordinate (2) or can be obtained by adopting Eulerian CFD models explained in Section 2.2.

2.1.1. GPBE in Turbulent Flow. In turbulent flows, in which turbulence is caused by instabilities in the continuous phase, the velocity of the continuous phase $\mathbf{U}_\mathrm{c}(t, \mathbf{x})$ is a random vector field characterized by fluctuations, that result in fluctuations of the NDF defined previously. The direct solution of the GPBE/PBE, which resolves all the relevant length and time scales, is computationally expensive and cheaper solutions are often sought. One alternative is to define a Reynolds-averaged NDF $\langle f \rangle(t, \mathbf{x}, \boldsymbol{\xi}, \mathbf{u})$ over an infinitely large number of realizations of the continuous phase velocity $\mathbf{U}_\mathrm{c}$ (2) and derive the following equation:

$$\partial_t \langle f \rangle + \partial_{\mathbf{x}}(\mathbf{u} \langle f \rangle) + \partial_{\boldsymbol{\xi}}(\langle \mathbf{G} f \rangle) + \partial_{\mathbf{u}}(\langle \mathbf{A} f \rangle) = \langle \mathcal{S} \rangle, \tag{4}$$

leading to a Reynolds-averaged Navier-Stokes (RANS) multiphase formulation. The terms $\langle \mathbf{G} f \rangle$, $\langle \mathbf{A} f \rangle$ and $\langle \mathcal{S} \rangle$ are generally not closed because the relations describing the continuous and discontinuous events depend on the continuous phase velocity, $\mathbf{U}_\mathrm{c}$. The above-mentioned terms are usually expressed as the summation of a mean field contribution and an additional contribution due to fluctuations, the latter of which needs a closure approximation. For example, Drew used a kinetic equation describing the evolution of particles in turbulent flows to derive the Eulerian momentum balance equation, which includes a drag force due to the mean fields and an additional contribution, called turbulent dispersion force, due to turbulent fluctuations (9). It is noteworthy that spatial filtering (10) and Large Eddy Simulation (LES) based on self-conditioned NDF (11) can be also used to derive the GPBE of the same form of Equation 4.

Stokes number: defined as the ratio of the element relaxation time ($\tau_e = \frac{\rho_e d_e^2}{18 \mu_c}$) to the characteristic time of the continuous phase (τ_c)

2.2. Eulerian Computational Fluid Dynamics

This section describes three main Eulerian approaches for CFD simulation of multiphase flows. Generally, the applicability of CFD approaches depends on the multiphase properties, particularly those of disperse phase. As shown in **Figure 1**, two key factors in selection of appropriate method are Stokes number and volume fraction of disperse phase elements. Another important factor is polydispersity index (PDI), as illustrated by **Figure 2**.

2.2.1. Dusty Gas Model. When disperse phase elements are sufficiently small, i.e. very small Stokes number, their trajectories are perfectly dictated by the velocity field of the continuous phase, $\mathbf{U}_\mathrm{c}$ (12). Thus, it is valid to assume that the elements move with a velocity

equal to $\mathbf{U}_c$. In such cases, the multiphase system is represented with one single continuous phase, whose properties, e.g. density and viscosity, are the same as the continuous phase for dilute systems, otherwise are modified to consider the presence of disperse phase elements.

2.2.2. Mixture Model. As the Stokes number of elements increases, the elements move with a velocity that may differ from the one of the continuous phase. Under equilibrium assumption, the relative velocity between the disperse elements and the continuous phase can be expressed as an algebraic relation obtained from a force balance on the elements (usually drag and buoyancy forces). When the disperse system is dilute enough, one momentum balance equation is solved for the velocity of the continuous phase, and then the algebraic relation is used to calculate the velocity of the disperse phase. This model is referred to as equilibrium Eulerian approach (13). Instead, when the number density of elements is higher, the disperse system is represented as one mixture fluid, for which a momentum balance equation is solved. This balance equation requires the knowledge of the relative velocities, which are specified by using the algebraic relation. This approach is known as the Mixture model (MM) (14, 15). An advantage of MM is the possibility of taking into account the polydispersity of multiphase systems by dividing the disperse elements into groups based on an internal coordinate, e.g. size of elements. Then, the relative velocity between each group (fluid) and the continuous phase can be expressed separately, which eventually depends on the selected internal coordinate of elements.

2.2.3. Two and Multi-fluid Models. The governing equations of Eulerian two-fluid model (TFM) can be derived from the GPBE, see **Figure 3**. The derivation is omitted here and it can be found elsewhere (2). For the sake of brevity, we report here only the mass and momentum balance equations for the continuous and disperse phases ($i = \mathrm{c}, \mathrm{d}$):

$$\partial_t(\rho_i \varepsilon_i) + \partial_{\mathbf{x}}(\rho_i \varepsilon_i \mathbf{U}_i) = 0 \tag{5}$$

$$\partial_t(\rho_i \varepsilon_i \mathbf{U}_i) + \partial_{\mathbf{x}}(\rho_i \varepsilon_i \mathbf{U}_i \mathbf{U}_i) = \partial_{\mathbf{x}}(\varepsilon_i \boldsymbol{\tau}_i) - \varepsilon_i \partial_{\mathbf{x}} p + \rho_i \varepsilon_i \mathbf{g} + \mathbf{M}_i \tag{6}$$

where ρ_i, ε_i and $\boldsymbol{\tau}_i$ denote the density, volume fraction and stress tensor of the phase i and p is the pressure (generally assumed the same for the continuous and disperse phases). The term $\mathbf{M}_i$ represents the momentum exchange between the continuous and disperse phases due to interfacial forces, such as drag and lift, and is generally modelled by closure relationships. For the disperse phase, the stress tensor $\boldsymbol{\tau}_i$ represents the dispersion of the element velocity ($\mathbf{u}$) around the mean disperse phase velocity ($\mathbf{U}_\mathrm{d}$). If the Stokes number of the elements is low enough, this stress tensor can be neglected, otherwise it is necessary to solve transport equations for higher-order moments of the disperse elements velocity (2). For the continuous phase, the stress tensor is modelled as for single-phase flows. When the flow is turbulent, the stress tensor of the continuous phase is generally closed by replacing the molecular viscosity with an effective one (16). The effective viscosity is the sum of the molecular viscosity and the turbulent viscosity, the latter of which is usually estimated by a two-equation model, e.g. $k-\varepsilon$ model, adapted for multiphase flows (17–20).

The TFM can be extended to consider more than two phases, e.g. dividing the disperse phase into several groups (fluids) based on the value of an internal coordinate (usually size). This approach, called Multi-fluid model (MFM), is particularly useful when the system under study is polydisperse, see **Figure 2**. The governing equations of MFM have similar shape as those of the TFM and can be found elsewhere (3, 4, 6, 7).

3. SOLUTION METHODS FOR PBE

Many methods are available in the literature for the numerical solution of PBEs, each has been developed to address the challenges posed by the application of interest. Some notable challenges include the number of internal coordinates, considering the element velocity as an internal coordinate (i.e. solving GPBE), and the physical and chemical phenomena involved. This section describes three principal categories of methods for the solution of PBEs. Among the ones not covered in this review, we should cite Monte Carlo methods (1, 2) that are currently too computationally expensive to be compatible with CFD coupling.

3.1. Class or Sectional Method (CM)

The class or sectional method is based on the discretization of the internal coordinate space into intervals (classes or sections), such that the PBE is transformed into a set of macroscopic balance equations in the physical domain (1). This method has been widely applied to polydisperse systems governed by a univariate PBE. Let the space of the generic internal coordinate ξ be divided into M intervals using $M+1$ grid points $(\xi_1, \xi_2, \ldots, \xi_{M+1})$, therefore, the i^{th} interval is defined as $I_i = [\xi_i, \xi_{i+1})$. The number density of elements in the interval I_i is given by $N_i(t, \mathbf{x}) = \int_{\xi_i}^{\xi_{i+1}} n(t, \mathbf{x}, \xi)\, \mathrm{d}\xi$, where $n(t, \mathbf{x}, \xi)$ is the NDF in Equation 1. Then, the discretized formulation of Equation 1 for the generic i^{th} interval is:

$$\partial_t N_i + \partial_{\mathbf{x}}(\mathbf{U}_i N_i) + \int_{\xi_i}^{\xi_{i+1}} \partial_\xi (Gn)\, \mathrm{d}\xi = \int_{\xi_i}^{\xi_{i+1}} \mathcal{S}\, \mathrm{d}\xi \tag{7}$$

where $\mathbf{U}_i$ is the velocity by which the elements of the i^{th} interval are transported in the physical space. The integrals in Equation 7 are not closed since they generally depend on the NDF and cannot be expressed in terms of N_i (1). A closed form of Equation 7 can be achieved by assuming a functional form for the NDF. Kumar and Ramkrishna (21) proposed a general procedure in which the NDF is approximated with the following form:

$$n(t, \mathbf{x}, \xi) = \sum_{i=1}^{M} N_i\, \delta(\xi - \zeta_i). \tag{8}$$

The above approximation implies that all the elements belonging to the interval i are concentrated at a pivotal point ζ_i inside the interval. Another common approximation assumes a constant number density in each interval, i.e. $n(t, \mathbf{x}, \xi) = N_i$ for $\xi_i < \xi < \xi_{i+1}$ (22). In the following, the procedure proposed by Kumar and Ramkrishna (21) is introduced without going into the full detail. For the sake of simplicity, the system is assumed to be homogeneous, i.e. no dependency on the physical space. Moreover, the contribution due the continuous changes is neglected at this stage and will be touched upon later.

In the case of aggregation and breakage, the RHS of Equation 7 can be written in the following closed form by assuming ξ to be a conserved property (1):

$$\begin{aligned} \int_{\xi_i}^{\xi_{i+1}} \mathcal{S}\, \mathrm{d}\xi = \frac{1}{2} \sum_{j=1}^{i-1} N_j \sum_{\substack{k \\ (\zeta_j + \zeta_k) \in I_i}} a(\zeta_j, \zeta_k)\, N_k \; - N_i \sum_{j=1}^{M} a(\zeta_i, \zeta_j)\, N_j \\ + \sum_{j=i}^{M} b(\zeta_j)\, N_j \int_{\xi_i}^{\xi_{i+1}} \beta(\xi | \zeta_j)\, \mathrm{d}\xi \; - b(\xi_i)\, N_i. \end{aligned} \tag{9}$$

Kumar and Ramkrishna (21) explained in detail that the above formulation is not internally consistent, i.e. it does not generally preserve the integral properties of the NDF such as its moments. It is noteworthy that low-order moments of the NDF are associated to the conserved properties of the disperse phase. The cause of this internal inconsistency lies in the assignment of a pivotal point to the born elements, produced by the birth (first and third) terms in Equation 9. For instance, let two elements belonging to the intervals I_j and I_k with pivotal points ζ_j and ζ_k coalesce to form a new element i with $\xi_i = \zeta_j + \zeta_k$. Then, the value ξ_i determines which interval the element i belongs to. However, in an arbitrarily discretized space, ξ_i may not necessarily coincide with the pivotal point of the assigned interval. The same issue may arise when an element breaks into two daughter elements, which should be assigned to two intervals. Kumar and Ramkrishna (21) proposed to assign the born elements to the nearby pivotal points, such that two integral properties of the NDF are preserved. This approach, known as the fixed-pivot approach, is quite general and is internally consistent, as far as two integral properties of the NDF are concerned (21). It is noteworthy that the number of conserved moments can be increased by distributing the born elements to more than two pivotal points as formulated by Alopaeus et al. (23).

Despite the competitive advantages of the fixed-pivot approach over previously developed approaches (24), Kumar and Ramkrishna (21) illustrated that the fixed-pivot approach overpredicts the NDF, particularly in case of aggregation/coalescence. They stated that the over-prediction issue arises due to the fixed pivotal points and proposed a new approach based on moving pivotal points. This method involves the solution for the number density (or a property of the NDF) at moving pivotal points, the location of which is governed by a differential equation. The locations of pivotal points change in such a way as to ensure preservation of the targeted properties. In another attempt to improve the predictions, a new technique was developed, called the cell-averaging technique, which assigns the born elements to the pivotal points on the basis of the average value of their internal coordinate (25). Numerical tests showed that the cell-averaging technique improves the results considerably (25). More details on this technique can be found elsewhere (25).

Concerning the continuous change of the internal coordinate, the third term on the LHS of Equation 7 can be written as follows:

$$\int_{\xi_i}^{\xi_{i+1}} \partial_\xi (Gn)\, \mathrm{d}\xi = (Gn)|_{\xi_{i+1}} - (Gn)|_{\xi_i}, \tag{10}$$

and it can be interpreted as the net flux of elements to/from the interval I_i, which is equal to the difference between the fluxes at the bounds of I_i. However, the NDF at the bounds of intervals is not known and must be approximated by interpolating the values at two neighbouring pivotal points. The upwind scheme is the simplest interpolation approach. Consider a generic bound ξ_i at which the number density $n(\xi_i)$ is needed. If the rate of continuous process at the bound $G(\xi_i)$ is positive, then $n(\xi_i) = N_{i-1}$, otherwise $n(\xi_i) = N_i$. The upwind scheme is first-order and therefore it suffers from numerical diffusion (2). Numerical diffusion can be avoided by integration over the characteristic curves (26), but this method is not suited for being incorporated in CFD codes. A more viable alternative is employing high-order schemes (27–29) which, however, do not guarantee the positivity of the N_i (26). To overcome this issue numerous methods have been proposed (1, 26)

Lastly, class or sectional methods can be extended to bi- and multi-variate PBE (30, 31). However, these extensions are not covered here as they are currently not compatible with CFD implementations because of their exceedingly large computational cost (16, 32, 33).

3.2. Method of Moments

The previous section mentioned several difficulties in tracking the evolution of the NDF through the direct solution of the PBE, which mainly arise due to the discretization of the internal coordinate space. In a pioneering work, Hulburt and Katz argued that the NDF contains too much information for many engineering applications and proposed an approximate system of description which tracks evolution of moments of the NDF instead of the NFD itself (34). In the most general form, the moments of the NDF are defined as:

$$\begin{aligned} m_{k_1,k_2,\ldots,k_d,k_{d+1},k_{d+2},k_{d+3}}(t,\mathbf{x}) &= \langle \xi_1^{k_1}\xi_2^{k_2}\ldots\xi_d^{k_d}u_1^{k_{d+1}}u_2^{k_{d+2}}u_3^{k_{d+3}}\rangle \\ &= \int_{\Omega_{\boldsymbol{\xi}}}\int_{\Omega_{\mathbf{u}}} \xi_1^{k_1}\xi_2^{k_2}\ldots\xi_d^{k_d}u_1^{k_{d+1}}u_2^{k_{d+2}}u_3^{k_{d+3}}\, f(t,\mathbf{x},\boldsymbol{\xi},\mathbf{u})\,\mathrm{d}\boldsymbol{\xi}\,\mathrm{d}\mathbf{u}, \end{aligned} \tag{11}$$

where $\mathbf{k} = (k_1, k_2, \ldots, k_d, k_{d+1}, k_{d+2}, k_{d+3})$ is the exponent vector. Each element of $\mathbf{k}$ is the order of the moment with respect to the corresponding internal coordinate or velocity component. The moments offer two key advantages which make the method of moments (MOM) attractive. Firstly, the moments are function of only time and space, i.e. they are Eulerian fields, and therefore an approach based on the moments is perfectly compatible to the solution methods readily available in CFD codes. The second advantage is that the low-order moments are related to some macroscopic properties of the disperse phase, which are physically meaningful and generally measurable. It is noteworthy that, in many applications, the ultimate aim of solving the PBE is to predict these macroscopic properties of the disperse phase.

A simplified example helps to elaborate on the subject without loss of generality. Let the internal coordinates comprise of the mass of the elements $\xi = M$ and the velocity. Then, the MOM involves the solution of a number of transport equations written in terms of the moments of the NDF. The moments $\langle \xi^0 u_1^0 u_2^0 u_3^0\rangle$, $\langle \xi^1 u_1^0 u_2^0 u_3^0\rangle$, and $\langle \xi^0 u_1^1 u_2^0 u_3^0\rangle$, $\langle \xi^0 u_1^0 u_2^1 u_3^0\rangle$ and $\langle \xi^0 u_1^0 u_2^0 u_3^1\rangle$ exemplify the importance of low-order moments since, they represent respectively: the total particle number density, the average particle mass density and the three components of the total particle momentum density.

The transport equation for a generic moment, $\langle \xi^{k_1} u_1^{k_2} u_2^{k_3} u_3^{k_4}\rangle$, is derived by multiplying the GPBE, Equation 3, with the function $g(\xi,\mathbf{u}) = \xi^{k_1} u_1^{k_2} u_2^{k_3} u_3^{k_4}$, and by integrating over the internal coordinate phase space:

$$\begin{aligned} &\partial_t\left(\int_{\mathbb{R}^+}\mathrm{d}\xi\int_{\mathbb{R}^3} gf\,\mathrm{d}\mathbf{u}\right) + \partial_{\mathbf{x}}\left(\int_{\mathbb{R}^+}\mathrm{d}\xi\int_{\mathbb{R}^3}\mathbf{u}gf\,\mathrm{d}\mathbf{u}\right) \\ &+ \int_{\mathbb{R}^+}\mathrm{d}\xi\int_{\mathbb{R}^3} g\,\partial_\xi(Gf)\,\mathrm{d}\mathbf{u} + \int_{\mathbb{R}^+}\mathrm{d}\xi\int_{\mathbb{R}^3} g\,\partial_{\mathbf{u}}(\mathbf{A}f)\,\mathrm{d}\mathbf{u} = \int_{\mathbb{R}^+}\mathrm{d}\xi\int_{\mathbb{R}^3} g\mathcal{S}\,\mathrm{d}\mathbf{u} \end{aligned} \tag{12}$$

The first term is the derivative of the moment with respect to time, $\partial_t\langle \xi^{k_1} u_1^{k_2} u_2^{k_3} u_3^{k_4}\rangle$. The second term is the moment transport in the physical space, which appears as the spatial derivative of a higher-order moment

$$\begin{aligned} \partial_{\mathbf{x}}\left(\int_{\mathbb{R}^+}\mathrm{d}\xi\int_{\mathbb{R}^3}\mathbf{u}gf\,\mathrm{d}\mathbf{u}\right) &= \partial_{x_1}\langle \xi^{k_1} u_1^{k_2+1} u_2^{k_3} u_3^{k_4}\rangle + \partial_{x_2}\langle \xi^{k_1} u_1^{k_2} u_2^{k_3+1} u_3^{k_4}\rangle \\ &\quad + \partial_{x_3}\langle \xi^{k_1} u_1^{k_2} u_2^{k_3} u_3^{k_4+1}\rangle, \end{aligned} \tag{13}$$

giving rise to the closure problem described in Section 3.2.1. The third term of the LHS of

Equation 12 can be simplified further by integration by part (2):

$$\int_{\mathbb{R}+} \mathrm{d}\xi \int_{\mathbb{R}^3} g\, \partial_\xi (Gf)\, \mathrm{d}\mathbf{u} = -\int_{\mathbb{R}^3} (gGf)|_{\xi=0}\, \mathrm{d}\mathbf{u} - \int_{\mathbb{R}+} \mathrm{d}\xi \int_{\mathbb{R}^3} \partial_\xi (g)\, Gf\, \mathrm{d}\mathbf{u}. \tag{14}$$

The first term on the RHS takes into account the appearance/disappearance of the disperse phase elements at the origin, which may be nonzero depending on the sign of G, i.e. if $g(\xi)$ is not zero and negative at the origin (2, 35). Likewise, the integration by part simplifies the fourth term of the LHS of Equation 12:

$$\int_{\mathbb{R}+} \mathrm{d}\xi \int_{\mathbb{R}^3} g\, \partial_{\mathbf{u}} (\mathbf{A}f)\, \mathrm{d}\mathbf{u} = -\int_{\mathbb{R}+} \mathrm{d}\xi \int_{\mathbb{R}^3} \mathbf{A}f\, \partial_{\mathbf{u}} (g)\, \mathrm{d}\mathbf{u}. \tag{15}$$

3.2.1. Closure Problem in MOM. The moment transport equations, i.e. Equation 12, are not in closed form, except few simple cases (2). One reason is that a set of transport equations written for a number of moments may contain terms which depend on higher-order moments. The addition of new moment transport equations for the higher-order moments would not solve the problem because the new equations give rise to new higher-order moments. On the other hand, the higher-order moments could be readily calculated if the NDF was known. In general, the knowledge of the NDF is also needed to calculate the source term and transport terms in the space of internal coordinate and velocity, see Equation 12. This is the main issue raised by the MOM, which is known as the closure problem. Several methods have been developed to close the moment transport equations, such as: interpolative closures (36), reconstruction of NDF with an assumed functional form (37–39) and approximating the NDF using a quadrature formula (40–42). The reader can find more details on developed closures in (2, 43). This work focuses on the closures based on the quadrature formula, known as Quadrature-based Moment Methods (QBMM), which has more general applicability in comparison to other proposed closures.

3.3. Quadrature-Based Moment Methods

In Quadrature-Based Moment Methods (QBMM) the NDF is approximated with an N-node quadrature formula, i.e. a summation of N weighted kernel density functions, each centered on a node/abscissa of a Gaussian quadrature approximation. The most commonly employed kernel density function is the Dirac delta function. The idea originated with McGraw (40), who employed an N-node Gaussian quadrature to approximate the integrals in the moment transport equations for the solution of a univariate PBE and named the approach quadrature method of moments (QMOM). The algorithm calculates the N abscissas and N weights of the quadrature from the $2N$ transported moments. In another work, Marchisio and Fox (42) developed a similar method, named direct quadrature method of moments (DQMOM), by which the quadrature approximation is transported in space and time such that the moments evolve according to the proper transport equations. In the following sections, both approaches are explained in detail. Moreover, the extension of QMOM to bi- and multi-variate PBE (i.e. conditional quadrature method of moments, CQMOM) will be also discussed. Lastly, an introduction will be given on the extended quadrature method of moments (EQMOM), which is useful in applications that require a continuous reconstruction of the NDF.

3.3.1. Quadrature Method of Moments. McGraw (40) proposed that the unclosed integrals of the moment transport equations can be approximated by employing an N-node

Gaussian quadrature formula. It is equivalent to assuming the following functional form to approximate the NDF (for a univariate problem):

$$n(t, \mathbf{x}, \xi) \approx \sum_{p=1}^{N} w_p(t, \mathbf{x})\, \delta[\xi - \xi_p(t, \mathbf{x})] \tag{16}$$

where $w_p(t, \mathbf{x})$ and $\xi_p(t, \mathbf{x})$ are the weight and abscissa of the node p. In the above expression, δ denotes the Dirac delta function. The moment of order k of the approximated NDF can be expressed as follows:

$$m_k = \int_{\mathbb{R}^+} \xi^k n(\xi)\, \mathrm{d}\xi \approx \sum_{p=1}^{N} w_p\, \xi_p^k \tag{17}$$

where m_k is an alternative notation for $\langle \xi^k \rangle$. The above relationship implies that knowledge about the first $2N$ moments enables us to determine the N weights and N abscissas of the quadrature approximation in Equation 16 by solving the following set of nonlinear equations:

$$m_0 = \sum_{p=1}^{N} w_p \quad , \quad m_1 = \sum_{p=1}^{N} w_p\, \xi_p^1 \quad , \quad \dots \quad m_{2N-1} = \sum_{p=1}^{N} w_p\, \xi_p^{2N-1}. \tag{18}$$

The above set of nonlinear equations are usually solved by employing well-conditioned recursive inversion algorithms such as the product-difference (PD) algorithm (44) and the Wheeler algorithm (45). The latter has the advantage of being applicable to distributions with zero mean value, i.e. $m_1 = 0$ in contrast to the PD algorithm (2). It is noteworthy that the weights and abscissas obtained from the solution of Equation 18 reproduce exactly the moments up to order $2N - 1$.

QMOM employs an N-node quadrature approximation to solve the transport equations for a set of moments of a PBE. The procedure of QMOM can be explained by writing the transport equation of a generic moment of order k derived from the PBE (Equation 1):

$$\partial_t(m_k) \, + \, \partial_{\mathbf{x}}(\mathbf{U}_{\mathrm{d},k} m_k) = \delta_{k,0}\, G(0)\, n(0) \, + \, k \int_{\mathbb{R}^+} \xi^{k-1}\, G n\, \mathrm{d}\xi + \int_{\mathbb{R}^+} \xi^k \mathcal{S}\, \mathrm{d}\xi, \tag{19}$$

where $\delta_{k,0}$ is the Kronecker delta and $\mathbf{U}_{\mathrm{d},k}$ denotes the transport velocity of the k-order moment defined by:

$$\mathbf{U}_{\mathrm{d},k} = \frac{1}{m_k} \int_{\mathbb{R}^+} \xi^k \mathbf{U}_{\mathrm{d}}(\xi)\, n\, \mathrm{d}\xi. \tag{20}$$

The first term on the RHS of Equation 19 appears only in the transport equation of the zeroth-order moment. This term is particularly challenging in the case of negative G, or in other words when the disperse phase elements are shrinking and disappearing. More detailed discussion on the subject can be found in (6, 46). In the latter reference, a method is suggested to reconstruct a continuous NDF by using the maximum entropy maximization, which enables the evaluation of the NDF at the origin (i.e. $\xi = 0$). In addition, a robust and efficient quadrature-based method was developed by Yuan and coworkers (47) to reconstruct a continuous NDF, see Section 3.3.4. The second term on the RHS of Equation 19 can be approximated using the N-node Gaussian quadrature formula:

$$k \int_{\mathbb{R}^+} \xi^{k-1}\, G(\xi) n(\xi)\, \mathrm{d}\xi \approx k \sum_{p=1}^{N} w_p \xi_p^{k-1} G(\xi_p). \tag{21}$$

The source term in the case of aggregation/coalescence and breakage is approximated likewise (assuming that ξ is a conserved property such as mass or volume of elements) (2):

$$\begin{aligned}\int_{\mathbb{R}^+} \xi^k \mathcal{S}\,\mathrm{d}\xi \approx \frac{1}{2}\sum_{p=1}^{N} w_p \sum_{q=1}^{N} (\xi_p+\xi_q)^k a(\xi_p,\xi_q)\, w_q - \sum_{p=1}^{N} \xi_p^k\, a(\xi_p,\xi_q)\, w_p \\ + \sum_{p=1}^{N} \left(\int_{\mathbb{R}^+} \xi^k \beta(\xi|\xi_p)\,\mathrm{d}\xi\right) b(\xi_p)\, w_p - \sum_{p=1}^{N} \xi_p^k\, b(\xi_p)\, w_p.\end{aligned} \tag{22}$$

The weights and abscissas of the quadrature formula in Equations 21 and 22 are determined by inverting the first $2N$ moments. Therefore, it is necessary to track the evolution of the first $2N$ moments by solving the corresponding transport equations. At each time step, the quadrature formula is determined by means of an inversion algorithm, which uses the $2N$ transported moments available from the previous time step or the initial conditions. It is noteworthy that the inversion algorithm fails if the moments are not realizable, i.e. the moment set is not inside the moments space (see the side bar Moment Space). The realizability issue mainly occurs due to the numerical methods that deal with the discretized moment transport equations, which are not the same as the exact equations. This fact necessitates employing numerical methods that are designed to prevent the realizability issue (48–52).

In general, a quadrature formula with more nodes yields more accurate approximation of integrals in the moment transport equations and an approximation of higher quality for the NDF. On the other hand, a quadrature with more nodes means more moments to be tracked, hence the need for more computational resources. In addition, the recursive algorithms for the calculation of the weights and abscissas become less stable as the number of nodes increases, and convergence is difficult to be achieved for typically $N > 10$ (2). However, Marchisio and Fox (41, 53) showed that satisfactory predictions can be achieved by employing a quadrature approximation with $2 \leq N \leq 4$ for simple aggregation and breakage problems. Moreover, QMOM predictions have acceptably small overall error not only for the tracked moments but also for higher-order moments (41).

Concerning the bi- and multi-variate PBE, the main challenge is the determination of the weights and (multi-dimensional) abscissas of the quadrature from the mixed moments, since the PD or Wheeler algorithms are applicable only to univariate quadratures. The next section focuses on the extension of QMOM to such cases by using conditional moments.

3.3.2. Conditional Quadrature Method of Moments. This section deals with the application of QBMM to the solution of bi- and multi-variate PBE. Let the NDF be defined over the space ($\Omega_{\boldsymbol{\xi}}$) of d internal coordinates, $\boldsymbol{\xi} = (\xi_1, \xi_2, \ldots, \xi_d)$. Then, the NDF can be approximated with the following functional form:

$$n(t,\mathbf{x},\boldsymbol{\xi}) \approx \sum_{p=1}^{N} w_p(t,\mathbf{x})\, \boldsymbol{\delta}[\boldsymbol{\xi} - \boldsymbol{\xi}_p(t,\mathbf{x})]\ , \quad \boldsymbol{\delta}[\boldsymbol{\xi} - \boldsymbol{\xi}_p(t,\mathbf{x})] = \prod_{\alpha=1}^{d} \delta[\xi_\alpha - \xi_{\alpha;p}(t,\mathbf{x})] \tag{23}$$

where $w_p(t,\mathbf{x})$ is the weight of the node p with abscissas $\boldsymbol{\xi}_p = (\xi_{1;p}, \xi_{2;p}, \ldots, \xi_{d;p})$ located in the joint space of the internal coordinates. The reader should bear in mind that the above quadrature is not a Gaussian quadrature. Moreover, univariate inversion methods such as PD or Wheeler algorithms are not applicable to multi-variate density functions.

The moments of the above approximation can be expressed as follows:

$$\langle \xi_1^{k_1} \xi_2^{k_2} \dots \xi_d^{k_d} \rangle = m_{k_1,k_2,\dots,k_d} = \sum_{p=1}^{N} w_p \prod_{\alpha=1}^{d} \xi_{\alpha;p}^{k_\alpha}. \tag{24}$$

The closure problem can be overcome by determining the quadrature approximation of order N, defined by N weights and N d-dimensional abscissas/nodes. The weights and abscissas of the quadrature nodes can be found by using a set of $N(d+1)$ moments. The inversion approach is desired to have some main properties of univariate inversion algorithms (2).

Firstly, it should be non-iterative otherwise its application to practical CFD simulations will be computationally expensive. Secondly, it should construct a mathematically and physically meaningful quadrature approximation – in other words, abscissas located in the support of the internal coordinates and non-negative weights. Lastly, the weights and abscissas obtained from the moments of an N-point density function should represent exactly the same N-point density function. Several methods have been developed to determine the high-dimensional quadrature points, such as the brute-force algorithm (54), the tensor-product algorithm (55–58) and the conditional quadrature method of moments (CQMOM) (59, 60), just to cite the most popular. Only the last method is discussed here since it is generally more stable and accurate.

For the sake of brevity, the explanation focuses on bi-variate NDF. The extension of the following procedure to more than two internal coordinates can be found in (2). In addition, the application of CQMOM to the kinetic equations, i.e. three velocity components as the internal coordinates, is discussed by Yuan and Fox (60). In CQMOM, the NDF is approximated by the following functional form:

$$n(t,\mathbf{x},\boldsymbol{\xi}) \approx \sum_{p_1=1}^{N_1} \sum_{p_2=1}^{N_2} w_{p_1}(t,\mathbf{x})\, w_{p_2,p_1}(t,\mathbf{x})\, \delta[\xi_1 - \xi_{1;p_1}(t,\mathbf{x})]\, \delta[\xi_2 - \xi_{2;p_2,p_1}(t,\mathbf{x})], \tag{25}$$

where w_{p_1} and $\xi_{1;p_1}$ are the weights and abscissas calculated from the pure moments with respect to the first internal coordinate (ξ_1) by using a univariate inversion algorithm. Instead, w_{p_2,p_1} and $\xi_{2;p_2,p_1}$ are the conditional weights and abscissas to be obtained by conditioning the second internal coordinate (ξ_2) on each abscissa of the first one ($\xi_{1;p_1}$). The calculation of the conditional weights and abscissas exploits the relationship between the mixed moments and the conditional NDF ($n_{2|1}$). First, the conditional NDF is defined by:

$$n_{2|1}(\xi_2|\xi_1) = \frac{n(\xi_1,\xi_2)}{n_1(\xi_1)}, \tag{26}$$

where $n_1(\xi_1) = \int_{\Omega_{\xi_2}} n(\xi_1,\xi_2)\,\mathrm{d}\xi_2$ is the marginal NDF of ξ_1. The moments of $n_1(\xi_1)$ are the same as the pure moments of $n(\xi_1,\xi_2)$ with respect to ξ_1 and therefore can be expressed in terms of w_{p_1} and $\xi_{1;p_1}$. Then, the mixed moments can be written as follows:

$$\begin{aligned} m_{k_1,k_2} &= \int_{\Omega_{\xi_1}} \xi_1^{k_1} n_1(\xi_1)\,\mathrm{d}\xi_1 \int_{\Omega_{\xi_2}} \xi_2^{k_2} n_{2|1}(\xi_2|\xi_1)\,\mathrm{d}\xi_2 \\ &= \sum_{p_1=1}^{N_1} w_{p_1} \xi_{1;p_1}^{k_1} \int_{\Omega_{\xi_2}} \xi_2^{k_2} n_{2|1}(\xi_2|\xi_{1;p_1}^{k_1})\,\mathrm{d}\xi_2 = \sum_{p_1=1}^{N_1} w_{p_1} \xi_{1;p_1}^{k_1} \langle \xi_2^{k_2} \rangle (\xi_{1;p_1}), \end{aligned} \tag{27}$$

where $\langle \xi_2^{k_2} \rangle (\xi_{1;p_1})$ denotes the conditional moments. Using the above relationship, the $N_1(2N_2-1)$ conditional moments can be obtained from the solution of the linear systems

of the following form written for $k_2 = 0, ..., 2N_2 - 1$:

$$\begin{bmatrix} 1 & \dots & 1 \\ \xi_{1;1} & \dots & \xi_{1;N_1} \\ \vdots & \ddots & \vdots \\ \xi_{1;1}^{N_1-1} & \dots & \xi_{1;N_1}^{N_1-1} \end{bmatrix} \begin{bmatrix} w_1 & & \\ & w_2 & \\ & & \ddots \\ & & & w_{N_1} \end{bmatrix} \begin{bmatrix} \langle \xi_2^{k_2} \rangle (\xi_{1;1}) \\ \langle \xi_2^{k_2} \rangle (\xi_{1;2}) \\ \vdots \\ \langle \xi_2^{k_2} \rangle (\xi_{1;N_1}) \end{bmatrix} = \begin{bmatrix} m_{0,k_2} \\ m_{1,k_2} \\ \vdots \\ m_{N_1-1,k_2} \end{bmatrix}. \quad (28)$$

The above linear system of equations, known as Vandermonde linear system, is non-singular as long as the abscissas $\xi_{1;p1}$ are distinct. The reader is referred to (61) for an efficient algorithm to solve the linear systems of the Vandermonde form. Finally, for each $\xi_{1;p1}$ a univariate inversion algorithm is applied to the corresponding set of conditional moments to find the corresponding conditional weights (w_{p_2,p_1}) and abscissas ($\xi_{2;p_2,p_1}$). Although the pure moments can be kept realizable by employing an appropriate numerical scheme, the realizability of the conditional moments is not guaranteed. In this case, the realizability issue can be overcome by applying the 1-D adaptive quadrature technique proposed by Yuan and Fox (60). With this technique, the maximum number of conditional moments belonging to the moment space is determined and consequently, the number of nodes for the second internal coordinate (at each $\xi_{1;p1}$) is adjusted accordingly.

One should pay attention to the selected order of internal coordinates conditioning as it changes the set of controlled moments (i.e. moments used in the reconstruction of the NDF). Nevertheless, all the moments controlled in CQMOM belong to the optimal moment set; see Section 3.3.3 for the definition and importance of such set.

3.3.3. Direct Quadrature Method of Moments. The direct quadrature method of moments (DQMOM) was first introduced by Marchisio and Fox (42) to avoid the need for an inversion algorithm, particularly in the case of bi/multi-variate problems. Although the inversion of moments in bi/multi-variate problems was later overcome by CQMOM, DQMOM has received considerable attention from the scientific community. Furthermore, DQMOM can be applied to univariate problems.

In contrast to QMOM and CQMOM, DQMOM employs transport equations written in terms of the weights w_p and weighted abscissas $\varsigma_{\alpha;p} = w_p \xi_{\alpha;p}$. Therefore, there is no need to employ an inversion algorithm except for the initialization of the weights and abscissas according to the initial conditions of the moments. Let the NDF be defined over the space of two internal coordinates and governed by the following bi-variate PBE:

$$\partial_t n + \partial_{\mathbf{x}}(\langle \mathbf{u} | \xi_1, \xi_2 \rangle n) + \partial_{\xi_1}(G_1 n) + \partial_{\xi_2}(G_2 n) = \int \mathcal{S} \, \mathrm{d}\mathbf{u}. \quad (29)$$

DQMOM approximates the NDF with the functional form in Equation 23. Then, the following transport equations can be written for the weights and weighted abscissas (42):

$$\begin{aligned} \partial_t w_p + \partial_{\mathbf{x}}(\langle \mathbf{u} \rangle_p w_p) &= s_p^w \\ \partial_t(\varsigma_{1;p}) + \partial_{\mathbf{x}}(\langle \mathbf{u} \rangle_p \varsigma_{1;p}) &= s_{1,p}^{\varsigma} \\ \partial_t(\varsigma_{2;p}) + \partial_{\mathbf{x}}(\langle \mathbf{u} \rangle_p \varsigma_{2;p}) &= s_{2,p}^{\varsigma} \end{aligned} \quad (30)$$

where $\langle \mathbf{u} \rangle_p = \langle \mathbf{u} | \xi_{1,p}, \xi_{2,p} \rangle$ denotes the velocity of the quadrature node p, and s_p^w, $s_{1,p}^{\varsigma}$ and $s_{1,p}^{\varsigma}$ are the source terms of the transport equations to be determined. The unknown source terms can be found by first replacing the NDF in Equation 29 with the functional

form in Equation 23 specialized for a bi-variate problem and then by applying the moment transformation of a generic order $\mathbf{k} = (k_1, k_2)$ (42):

$$\sum_{p=1}^{N}(1-k_1-k_2)\xi_{1,p}^{k_1}\xi_{2,p}^{k_2}s_p^w - \sum_{p=1}^{N}k_1\xi_{1,p}^{k_1-1}\xi_{2,p}^{k_2}s_{1,p}^{\varsigma} + \sum_{p=1}^{N}k_2\xi_{1,p}^{k_1}\xi_{2,p}^{k_2-1}s_{2,p}^{\varsigma} = \bar{h}_{k_1,k_2}, \qquad (31)$$

where $\bar{h}_{k_1,k_2}$ takes into account the change of the moment due to the continuous and discontinuous events and therefore is problem dependent. A system of $3N$ linear equations (equal to the number of unknowns) can be formed by writing Equation 31 for $3N$ moments of different order. The solution of the linear system can be expressed in the matrix form $\mathbf{s} = \mathcal{A}^{-1}\mathbf{h}$, where $\mathbf{s} = [s_1^w \dots s_N^w \; s_{1,1}^{\varsigma} \dots s_{1,N}^{\varsigma} \; s_{2,1}^{\varsigma} \dots s_{2,N}^{\varsigma}]^T$ and $\mathcal{A}$ is the coefficient matrix. The matrix $\mathcal{A}$ should be non-singular and therefore requires some considerations. Firstly, the abscissas must remain distinct in order to prevent singularity. Thus, using too many nodes is not recommended since the probability of two nodes approaching each other increases by adding more nodes (2). Another important point is the choice of the moment set, which is studied by Fox in detail (62). Fox established a methodology to choose a set of moments, called optimal moment set, that results in a non-singular coefficient matrix $\mathcal{A}$. Eventually, the optimal moment sets for problems with $1 \leq d \leq 3$ were reported. The concept was developed by using $N = r^d$ nodes for $r \in \mathbb{Z}_{>0}$, which treats all the internal coordinates equally. It is noteworthy to mention the possibility of choosing other moments, which result yet in a valid but not optimal set. However, one should try to use a moment set that covers the important moments, i.e. those with physical significance, and that includes enough mixed moments to avoid losing the correlation between the internal coordinates. For more details, the reader is referred to the discussion of choosing the moment set in (2).

3.3.4. Extended Quadrature Method of Moments. The previous QBMM approximate the NDF with an N-point discontinuous distribution, i.e. a summation of N weighted Dirac delta functions. However, some applications require a continuous reconstructed NDF to correctly model the phenomena involved, e.g. evaporating sprays (46). Yuan et al. (47) suggested a method, called extended quadrature method of moments (EQMOM), which employs a parametric continuous kernel density function (KDF) instead of the Dirac delta function:

$$n(t, \mathbf{x}, \xi) \approx \sum_{p=1}^{N} w_p(t, \mathbf{x})\, \delta_\sigma[\xi; \xi_p(t, \mathbf{x})], \qquad (32)$$

where $\delta_\sigma(\xi; \xi_p)$ is a chosen KDF, which depends on the parameter σ. The weights and abscissas associated to the KDF are denoted by w_p and ξ_p. The determination of the parameter σ requires that one additional moment should be tracked, in comparison to the $2N$ moments tracked in QMOM. The KDF is required to reduce smoothly to the Dirac delta function in the limit of $\sigma \to 0$, meaning that the quadrature can be reconstructed from the first $2N$ moments when $\sigma = 0$. The choice of the KDF is problem dependent, i.e. the support of the KDF should be consistent with the support of the internal coordinate. Common KDF are Gaussian distribution with infinite support $(-\infty, \infty)$, gamma and log-normal distributions with semi-infinite positive support $[0, \infty)$ and beta distribution with finite support $[0, 1]$. Moreover, it is practically important that the selected KDF can be defined in terms of the weight function $w(\theta)$ for a known family of orthogonal polynomials. In the following, the algorithm for the calculation of the weights and abscissas of the quadrature approximation as well as the parameter σ will be explained for a univariate

NDF with semi-infinite positive support. The application of EQMOM to problems with infinite or finite supports is similar and can be found elsewhere (2, 47). In addition, the reader is referred to (2) for the extension of the EQMOM to multi-variate problems.

As mentioned previously, a suitable choice of KDF for problems with support of $[0, \infty)$ is the gamma distribution. Then, the NDF is approximated by the following summation of N weighted parameterized gamma distributions:

$$n(\xi) \approx \sum_{p=1}^{N} w_p \frac{\xi^{\lambda_p - 1} e^{-\xi/\sigma}}{\Gamma(\lambda_p)\sigma^{\lambda_p}} \quad \text{and} \quad \lambda_p(t, \mathbf{x}) = \frac{\xi_p}{\sigma}, \tag{33}$$

where Γ is the gamma function. The moments of the NDF can be expressed as:

$$m_k(t, \mathbf{x}) = \sum_{p=1}^{N} w_p \frac{\Gamma(\lambda_p + k)}{\Gamma(\lambda_p)} \sigma^k = \sum_{p=1}^{N} w_p \xi_p^k + \sum_{p=1}^{N} w_p P_{k-1}(\xi_p, \sigma), \tag{34}$$

where $P_{k-1}(\xi_p, \sigma)$ is a homogeneous polynomial of order $k-1$ with respect to ξ_p and σ. The summation $\sum_{p=1}^{N} w_p \xi_p^k$ is indeed the k^{th}-order moment of the quadrature in the limit $\sigma = 0$, and here is denoted by m_k^*. Equation 34 can be written for the first $2N+1$ moments to calculate the weights and abscissas as well as the parameter σ of the quadrature. An important observation is that the RHS of Equation 34 can be rewritten in terms of only m_k^* and σ. Subsequently, the two sets of moments $\mathbf{m} = (m_0, m_1, \ldots, m_{2N})$ and $\mathbf{m}^* = (m_0^*, m_1^*, \ldots, m_{2N}^*)$ can be related through the matrix form $\mathbf{m} = \mathbf{B}(\sigma)\mathbf{m}^*$. The matrix $\mathbf{B}(\sigma)$ is a lower-triangular matrix, which allows to calculate the moment m_k^* from the moments $(m_0, m_1, \ldots, m_k)$ for a given value of σ. Eventually, the following iterative approach can be used to determine the quadrature approximation (47):

1. Guess the parameter σ and calculate the first $2N$ moments $(m_0^*, m_1^*, \ldots, m_{2N-1}^*)$ using $\mathbf{m}^* = \mathbf{B}^{-1}(\sigma)\mathbf{m}$
2. Find the weights w_p and abscissas ξ_p from the moments $(m_0^*, m_1^*, \ldots, m_{2N-1}^*)$ by employing the adaptive quadrature algorithm,
3. Use the weights and abscissas to calculate $m_{2N}^* = \sum_{p=1}^{N} w_p \xi_p^{2N}$,
4. Calculate the scalar function $J(\sigma) = m_{2N} - m_{2N}^* - \sum_{p=1}^{N} w_p P_{2N-1}(\xi_p, \sigma)$
5. Guess a new σ until the convergence $J(\sigma) = 0$ is achieved for the smallest σ.

In the above approach, the adaptive quadrature algorithm allows to cope with the non-realizable set of moments. Once the quadrature is determined, it can be used to close the terms appearing in the moment transport equations, i.e. Equation 32. For this purpose, a general integral of the NDF is considered:

$$\int_{\Omega_\xi} g(\xi) n(\xi)\, \mathrm{d}\xi = \sum_{p=1}^{N} w_p \int_{\Omega_\xi} g(\xi) \delta_\sigma(\xi; \xi_p)\, \mathrm{d}\xi = \sum_{p=1}^{N} \sum_{q=1}^{N'} w_p w_q^{(p)}\, g(\xi_q^{(p)}), \tag{35}$$

where $g(\xi)$ is a generic function of the internal coordinate. In Equation 35, the integral of the KDF $\delta_\sigma(\xi; \xi_p)$ is approximated by a quadrature formula, for which the weights $w_q^{(p)}$ and abscissas $\xi_q^{(p)}$ can be calculated from the recursion coefficients that are known in advance. Moreover, the number of nodes of the second quadrature (N') does not depend on N and can be increased independently to improve the accuracy.

3.4. Selection of the Solution Method

A key factor in selection of the solution method is the number of internal coordinates. For univariate problems, CM and QMOM are regarded as the first candidates. The CM is more suitable for simulation of systems in which the NDF can be measured directly. On the other hand, QMOM provides information about some (usually measurable) integral properties of the NDF. From the computational point of view, QMOM is normally less demanding than CM. In fact, achieving a reasonable accuracy by the CM generally requires a large number of intervals/classes which is computationally expensive, particularly when disperse phase elements span over a wide region of the phase space (41). Therefore, QMOM is the preferred method for the CFD simulation of spatially heterogeneous systems, specifically those of large-scale (5). Furthermore, the CM should use high-order schemes when the system under study involves continuous events, in particular if the number of intervals cannot be increased sufficiently. However, employing high-order schemes usually lead to instabilities. On the other hand, QBMM handle continuous events easily, if the growth rate is positive. In case of negative growth rates, i.e. evaporation/dissolution, EQMOM can be used to estimate the value of the NDF at the origin of the relevant internal coordinate. Moreover, EQMOM should be generally used when the particulate processes of interest are highly localized in the phase space (63). In fact, with other QBMM, some phenomena may be ignored if there is no node/abscissa in the region where they are active. Furthermore, the addition of nodes does not necessarily improve the situation as QMOM shows unpredictable behaviour in response to the increase in the number of nodes, when highly localized phenomena are present (63). In such cases, the CM or EQMOM are more appropriate.

In the case of bi- and multi-variate PBE, QBMM are generally the preferred methods. Both DQMOM and CQMOM were developed to overcome the difficulties of moment inversion in bi- and multi-variate problems. However, CQMOM has some advantages over DQMOM. Firstly, the equivalence between DQMOM and QMOM/CQMOM is lost in pure hyperbolic PBE (2), in contrast to spatially homogeneous systems. Moreover, DQMOM is not valid for purely hyperbolic PBE in the presence of (spatial or time) discontinuity in the weights and abscissas, because the transport equations in Equation 30 are derived on the assumption that the weights and abscissas are continuous function of time and space (2). Another point is that DQMOM does not guarantee the conservation of the moments except for the moment of order zero and one, and needs corrective terms to respect the conservation of the moments of higher-order (2). Lastly, when a continuous NDF is needed, CQMOM can be extended to use a KDF other than the Dirac delta function, i.e. the extended conditional quadrature method of moments (2).

4. Implementation in CFD

As mentioned previously, the solution of the GPBE/PBE provides detailed information about the disperse phase, which can result in a more accurate solution. For instance, a more accurate estimation of the drag force can be obtained by using the instantaneous size distribution of the disperse phase elements instead of a fixed constant element size. At the same time, the solution of the GPBE/PBE requires knowledge of the flow fields. Therefore, it is necessary to adopt a suitable approach to couple CFD and GPBE/PBE, as explained in the following section.

4.1. Monokinetic Models

Monokinetic models, e.g. TFM and MFM, assume zero velocity dispersion around the mean velocity (or mean velocities) of elements located at the same spatial coordinates at a given time and characterized by the same internal coordinate values. This assumption is valid for elements with small Stokes numbers (St $<$ 1) (13). Within this context, the simplest approach assigns one velocity, $\mathbf{U}_{\mathrm{d}}(t, \mathbf{x})$, to all elements of the disperse phase, which depends only on the spatial coordinates and time and not on the internal coordinates. The common methods for obtaining the velocity of the disperse phase, required to solve the PBE, include MM and TFM (5, 32, 64–71), although the dusty gas approach (72) and the equilibrium Eulerian approach (13) can be used for sufficiently small elements (12). At the same time, the polydispersity of the elements will be described through the solution of the PBE, Equation 1, by using a suitable method described in the previous section. When the CM is used to solve the PBE, the coupling terms are evaluated using the properties of each class of disperse elements. On the other hand, in case of adopting QMOM, it is possible to calculate the coupling terms by using either the average properties of the disperse elements, which are associated to the moments, or the quadrature nodes separately (16).

The assumption of identical element velocity can be relaxed partially by employing a multi-fluid approach, where the elements are grouped into several phases based on the value of an internal coordinate (usually size). When the CM is chosen to solve the PBM (3, 65, 73–75), each class is assumed to move with its own velocity. In the case of QMOM or DQMOM (5, 8, 76, 77), each node of the quadrature moves with a unique velocity. The velocity of each class (or node in case of QMOM or DQMOM) is obtained either by solving a momentum balance equation written for the corresponding class (or node) or by adopting the MM, see Section 2.2.

Particle trajectory crossing (PTC): In dilute systems, particles of different velocity (regardless of their properties) can cross each other without collision

The monokinetic assumption is not valid in case of elements with large Stokes numbers, since large elements do not adapt quickly to the surrounding fluid velocity and therefore the effect of their initial conditions lasts for a long time (13). For instance, this assumption may lead to nonphysical predictions in dilute systems comprises of particles characterized with large Stokes number, where particle trajectory crossing (PTC) can occur (48, 57). A possible approach to describing such systems is adoption of a polykinetic model.

4.2. Polykinetic Models

It is necessary to include the element velocity as an internal coordinate, when dealing with disperse systems far from equilibrium or comprised of elements characterized by very large Stokes numbers. In such cases, the evolution of the disperse phase in space and time is entirely governed by the GPBE, Equation 3, while the continuous phase is described by Equations 5 and 6. The interaction between the phases is taken into account through the exchange terms in the governing equations of both phases. The quadrature-based methods are preferred to solve the GPBE since the application of the CM to this equation is not tractable. In this regard, the QMOM, DQMOM and specifically CQMOM are promising tools to solve the GPBE (2, 6, 48, 57–60).

When the disperse system is very dilute, the effect of the disperse phase on the flow field of the continuous phase can be assumed negligible (2, 78). Thus, one-way coupling suffices to consider the effect of the continuous phase on the evolution of the disperse phase elements. The flow fields of the continuous phase are predicted by the solution of the single-phase Navier-Stokes equations. At each time-step, the governing equations of the

continuous phase are solved to predict the flow fields of the continuous phase, which will be eventually used to estimate the closure relations in the GPBE. It is possible to advance the GPBE with several smaller time-steps within each time-step of the CFD solver, if the time-scale of the phenomena affecting the elements is comparably smaller than the characteristic time-scale of the continuous phase (78).

On the other hand, the effect of disperse elements on flow fields of the continuous phase becomes significant as the number density of elements increases. Thus, governing equations of the continuous phase should include exchange terms due to the presence of the disperse phase elements, e.g. Equations 5 and 6 (79, 80). Convergence issues may arise in the two-way coupling due to the explicit exchange terms included in the governing equations. For instance, the drag force generally depends on the relative velocity of the phases and, if handled explicitly, hinders convergence. The convergence rate can be improved by adopting the partial elimination algorithm (81). The application of partial elimination algorithm to CFD-QMOM simulations is explained by Passalacqua and co-workers (78, 79).

4.3. Numerical Issues of QBMM

Efficient numerical methods for solving the PBE must provide sufficiently accurate solutions as well as ensure the stability of the simulation. A major reason of simulation instabilities is the appearance of non-physical solutions during the simulation, i.e. the realizability issue associated to the QBMM. The realizability issue appears mostly when standard high-order schemes are employed for the independent advection of the moments (82). These schemes aim mainly at achieving high-order and oscillation-free solutions for transported variables. However, the moments are linked variables which belong to the moment space, therefore, a selected numerical scheme must additionally ensure that the moment space is preserved. Unfortunately, only 1^{st}-order schemes, e.g. upwind scheme, are guaranteed to yield realizable moment sets provided that the Courant–Friedrichs–Lewy (CFL) condition is satisfied (48). It is noteworthy that the CFL condition generally serves as the criterion for the stability of the CFD simulations. The 1^{st}-order schemes, albeit being very stable, generally produce diffused solutions for computationally affordable grid sizes. Therefore, if high-order solutions are required, one must employ high-order schemes which are specifically designed to overcome the realizability issue.

High-resolution (HR) TVD schemes: interpolation schemes that employ a flux limiter to prevent oscillations in the solution of hyperbolic problems (83, 84)

In a pioneer work, Vikas and coworkers proposed the quasi-high-order realizable schemes, which interpolates separately the weights and abscissas of the quadrature (instead of the moments) from the cell centers to the faces (49). In this approach, the quadrature weights on the faces are obtained with a high-resolution (HR) total variation diminishing (TVD) scheme whereas the quadrature abscissas on the faces are obtained by using the 1^{st}-order upwind scheme. With this technique, the realizability issue is avoided if a criterion for the time-step is fulfilled (49). This approach can be applied for the solution of both PBE and GPBE. Moreover, it can be simply implemented in CFD codes, regardless of the spatial dimensionality and mesh type. Another notable approach preserves the moment space by advecting a sequence of positive variables, called ζ-variable, which are connected to the moments (51). The application of the original version of this approach to arbitrary unstructured grids is not straightforward. Nevertheless, Passalacqua and coworker extended the applicability of this approach to unstructured meshes (85).

In addition to the realizability issue, the boundedness of the solution is another important numerical aspect because the low-order moments are associated to some average

physical properties of the elements, which are bounded in nature (86). This aspect should be considered in the selection of the numerical solution method if bounded solution for the moments is desired. For instance, Shiea and coworkers observed oscillations in the solution for the advection of moments in a one-dimensional Riemann problem obtained by using a quasi-high-order realizable scheme (52). They argued that oscillation-free solution for the moments is not necessarily guaranteed when the HR TVD schemes are not applied directly to the moments. Eventually, they suggested that it is possible to apply the HR TVD schemes directly to the moments without encountering the realizability issue by using an identical limiter (equal-limiter) for all the transported moments (52). They additionally showed that the boundedness of the moments is guaranteed if the equal-limiter is set to the smallest limiter among those calculated independently for the transported moments.

5. CFD-PBE CODES

Apart from the numerous in-house codes reported in the literature, there are several commercial and open-source CFD codes, which incorporate the PBE. **Table 1** summarizes some available CFD-PBE codes along with their main features and related references.

SUMMARY POINTS

1. The governing equations for the Eulerian CFD-PBE simulation of disperse multiphase systems are described.
2. The common solution methods for the solution of the PBE are explained and a guideline is presented to select a suitable one.
3. When the Stokes number of elements is sufficiently small ($St < 1$), the monokinetic assumption is valid and the velocity of the disperse phase is predicted by a multiphase CFD solver. Otherwise, the GPBE governs the evolution of the distribution of the elements over the space of the internal properties, including the velocity.
4. In QBMM, the realizability issue is the main cause of simulation instability and can be addressed by adopting the numerical schemes mentioned in this review. In addition, particular attention should be paid to the boundedness of the solution of the moment transport equations, when realizable schemes are employed.
5. Some discussed approaches for the simulation of disperse multiphase systems are accessible through several available commercial and open-source CFD-PBE codes, from which the leading ones are reported in the paper.

FUTURE ISSUES

1. Despite the existing advances, the development of more robust numerical methods which increase simultaneously the accuracy and the stability of simulations, e.g. the realizable numerical schemes, continues to be an interesting subject.
2. It is fruitful to develop efficient CFD-PBE codes or contribute to improve the existing ones, particularly the open-source codes such as OpenQBMM project (https://www.openqbmm.org) (85). These codes expand the application of the PBE to vast relevant subjects spanning a broad scientific and industrial communities, which ultimately lead to rapid advances in different aspects of the PBE.

DISCLOSURE STATEMENT

The authors are not aware of any affiliations, memberships, funding, or financial holdings that might be perceived as affecting the objectivity of this review.

LITERATURE CITED

1. Ramkrishna D. 2000. Population balances: Theory and applications to particulate systems in engineering. Academic Press, 1st ed.
2. Marchisio DL, Fox RO. 2013. Computational models for polydisperse particulate and multiphase systems. Cambridge Series in Chemical Engineering. Cambridge, UK: Cambridge University Press
3. Laurent F, Massot M. 2001. Multi-fluid modelling of laminar polydisperse spray flames: origin, assumptions and comparison of sectional and sampling methods. *Combustion theory and modelling* 5:537–572
4. Laurent F, Massot M, Villedieu P. 2004. Eulerian multi-fluid modeling for the numerical simulation of coalescence in polydisperse dense liquid sprays. *Journal of Computational Physics* 194:505–543
5. Fan R, Marchisio DL, Fox RO. 2004. Application of the direct quadrature method of moments to polydisperse gas-solid fluidized beds. *Powder Technology* 139:7–20
6. Fox RO, Laurent F, Massot M. 2008. Numerical simulation of spray coalescence in an eulerian framework: direct quadrature method of moments and multi-fluid method. *Journal of Computational Physics* 227:3058–3088
7. De Chaisemartin S, Fréret L, Kah D, Laurent F, Fox R, et al. 2009. Eulerian models for turbulent spray combustion with polydispersity and droplet crossing. *Comptes Rendus Mécanique* 337:438–448
8. Mazzei L, Marchisio DL, Lettieri P. 2012. New quadrature-based moment method for the mixing of inert polydisperse fluidized powders in commercial CFD codes. *AIChE Journal* 58:3054–3069
9. Drew DA. 2001. A turbulent dispersion model for particles or bubbles. *Journal of Engineering Mathematics* 41:259–274
10. Zaichik L, Simonin O, Alipchenkov V. 2009. An Eulerian approach for large eddy simulation of particle transport in turbulent flows. *Journal of Turbulence* 10:1–21
11. Fox RO. 2012. Large-eddy-simulation tools for multiphase flows. *Annual Review of Fluid Mechanics* 44:47–76
12. Balachandar S, Eaton JK. 2010. Turbulent dispersed multiphase flow. *Annual Review of Fluid Mechanics* 42:111–133
13. Ferry J, Balachandar S. 2001. A fast eulerian method for disperse two-phase flow. *International Journal of Multiphase Flow* 27:1199–1226
14. Manninen M, Taivassalo V, Kallio S, et al. 1996. On the mixture model for multiphase flow
15. Sanyal J, Vásquez S, Roy S, Dudukovic M. 1999. Numerical simulation of gas–liquid dynamics in cylindrical bubble column reactors. *Chemical Engineering Science* 54:5071–5083
16. Buffo A, Marchisio DL. 2014. Modeling and simulation of turbulent polydisperse gas-liquid systems via the generalized population balance equation. *Reviews in Chemical Engineering* 30:73–126
17. Kataoka I, Serizawa A. 1989. Basic equations of turbulence in gas-liquid two-phase flow. *International Journal of Multiphase Flow* 15:843–855
18. Lopez de Bertodano MA, Saif AA. 1997. Modified $k-\varepsilon$ model for two-phase turbulent jets. *Nuclear Engineering and Design* 172:187–196

19. Peirano E, Leckner B. 1998. Fundamentals of turbulent gas-solid flows applied to circulating fluidized bed combustion. *Progress in Energy and Combustion Science* 24:259–296
20. Troshko A, Hassan Y. 2001. A two-equation turbulence model of turbulent bubbly flows. *International Journal of Multiphase Flow* 27:1965–2000
21. Kumar S, Ramkrishna D. 1996. On the solution of population balance equations by discretization–I. A fixed pivot technique. *Chemical Engineering Science* 51:1311–1332
22. Gelbard F, Tambour Y, Seinfeld JH. 1980. Sectional representations for simulating aerosol dynamics. *Journal of Colloid and Interface Science* 76:541–556
23. Alopaeus V, Laakkonen M, Aittamaa J. 2006. Solution of population balances with breakage and agglomeration by high-order moment-conserving method of classes. *Chemical Engineering Science* 61:6732–6752
24. Vanni M. 2000. Approximate population balance equations for aggregation-breakage processes. *Journal of Colloid and Interface Science* 221:143–160
25. Kumar J, Peglow M, Warnecke G, Heinrich S, Mörl L. 2006. Improved accuracy and convergence of discretized population balance for aggregation: The cell average technique. *Chemical Engineering Science* 61:3327–3342
26. Kumar S, Ramkrishna D. 1997. On the solution of population balance equations by discretization–III. Nucleation, growth and aggregation of particles. *Chemical Engineering Science* 52:4659–4679
27. Marchal P, David R, Klein J, Villermaux J. 1988. Crystallization and precipitation engineering–I. An efficient method for solving population balance in crystallization with agglomeration. *Chemical Engineering Science* 43:59–67
28. David R, Villermaux J, Marchal P, Klein JP. 1991. Crystallization and precipitation engineering–IV. kinetic model of adipic acid crystallization. *Chemical Engineering Science* 46:1129–1136
29. Hounslow M, Ryall R, Marshall V. 1988. A discretized population balance for nucleation, growth, and aggregation. *AIChE Journal* 34:1821–1832
30. Kumar J, Peglow M, Warnecke G, Heinrich S. 2008. The cell average technique for solving multi-dimensional aggregation population balance equations. *Computers & Chemical Engineering* 32:1810–1830
31. Buffo A, Alopaeus V. 2016. Solution of bivariate population balance equations with high-order moment-conserving method of classes. *Computers & Chemical Engineering* 87:111–124
32. Buffo A, Vanni M, Marchisio DL, Fox RO. 2013. Multivariate quadrature-based moments methods for turbulent polydisperse gas-liquid systems. *International Journal of Multiphase Flow* 50:41–57
33. Buffo A, Marchisio DL, Vanni M, Renze P. 2013. Simulation of polydisperse multiphase systems using population balances and example application to bubbly flows. *Chemical Engineering Research and Design* 91:1859–1875
34. Hulburt HM, Katz S. 1964. Some problems in particle technology: A statistical mechanical formulation. *Chemical Engineering Science* 19:555–574
35. Fox RO. 2007. Introduction and fundamentals of modeling approaches for polydisperse multiphase flows. In *Multiphase Reacting Flows: Modelling and Simulation. CISM International Centre for Mechanical Sciences*, eds. DL Marchisio, RO Fox, vol. 492. Springer, 1–40
36. Frenklach M. 2002. Method of moments with interpolative closure. *Chemical Engineering Science* 57:2229–2239
37. Lee K. 1983. Change of particle size distribution during brownian coagulation. *Journal of Colloid and Interface Science* 92:315–325
38. Kruis FE, Kusters KA, Pratsinis SE, Scarlett B. 1993. A simple model for the evolution of the characteristics of aggregate particles undergoing coagulation and sintering. *Aerosol science and technology* 19:514–526
39. Strumendo M, Arastoopour H. 2008. Solution of PBE by MOM in finite size domains. *Chemical*

Engineering Science 63:2624–2640
40. McGraw R. 1997. Description of aerosol dynamics by the quadrature method of moments. *Aerosol Science and Technology* 27:255–265
41. Marchisio DL, Vigil RD, Fox RO. 2003. Quadrature method of moments for aggregation-breakage processes. *Journal of Colloid and Interface Science* 258:322–334
42. Marchisio DL, Fox RO. 2005. Solution of population balance equations using the direct quadrature method of moments. *Journal of Aerosol Science* 36:43–73
43. Diemer R, Olson J. 2002. A moment methodology for coagulation and breakage problems: Part 2–moment models and distribution reconstruction. *Chemical Engineering Science* 57:2211–2228
44. Gordon RG. 1968. Error bounds in equilibrium statistical mechanics. *Journal of Mathematical Physics* 9:655–663
45. Wheeler JC. 1974. Modified moments and gaussian quadratures. *Rocky Mountain Journal of Mathematics* 4:287–296
46. Massot M, Laurent F, Kah D, De Chaisemartin S. 2010. A robust moment method for evaluation of the disappearance rate of evaporating sprays. *SIAM Journal on Applied Mathematics* 70:3203–3234
47. Yuan C, Laurent F, Fox RO. 2012. An extended quadrature method of moments for population balance equations. *Journal of Aerosol Science* 51:1–23
48. Desjardins O, Fox RO, Villedieu P. 2008. A quadrature-based moment method for dilute fluid-particle flows. *Journal of Computational Physics* 227:2514–2539
49. Vikas V, Wang ZJ, Passalacqua A, Fox RO. 2011. Realizable high-order finite-volume schemes for quadrature-based moment methods. *Journal of Computational Physics* 230:5328–5352
50. Kah D, Laurent F, Massot M, Jay S. 2012. A high order moment method simulating evaporation and advection of a polydisperse liquid spray. *Journal of Computational Physics* 231:394–422
51. Laurent F, Nguyen TT. 2017. Realizable second-order finite-volume schemes for the advection of moment sets of the particle size distribution. *Journal of Computational Physics* 337:309–338
52. Shiea M, Buffo A, Vanni M, Marchisio D. 2018. A novel finite-volume TVD scheme to overcome non-realizability problem in quadrature-based moment methods. *submitted to Journal of Computational Physics*
53. Marchisio DL, Soos M, Sefcik J, Morbidelli M. 2006. Role of turbulent shear rate distribution in aggregation and breakage processes. *AIChE journal* 52:158–173
54. Wright Jr. DL, McGraw R, Rosner DE. 2001. Bivariate extension of the quadrature method of moments for modeling simultaneous coagulation and sintering of particle populations. *Journal of Colloid and Interface Science* 236:242–251
55. Yoon C, McGraw R. 2004. Representation of generally mixed multivariate aerosols by the quadrature method of moments: I. statistical foundation. *Journal of Aerosol Science* 35:561–576
56. Yoon C, McGraw R. 2004. Representation of generally mixed multivariate aerosols by the quadrature method of moments: II. aerosol dynamics. *Journal of Aerosol Science* 35:577–598
57. Fox RO. 2008. A quadrature-based third-order moment method for dilute gas-particle flows. *Journal of Computational Physics* 227:6313–6350
58. Fox RO. 2009. Higher-order quadrature-based moment methods for kinetic equations. *Journal of Computational Physics* 228:7771–7791
59. Cheng JC, Fox RO. 2010. Kinetic modeling of nanoprecipitation using CFD coupled with a population balance. *Industrial & Engineering Chemistry Research* 49:10651–10662
60. Yuan C, Fox RO. 2011. Conditional quadrature method of moments for kinetic equations. *Journal of Computational Physics* 230:8216–8246
61. Press WH, Teukolsky SA, Vetterling WT, Flannery BP. 2007. Numerical recipes: The art of scientific computing. Cambridge University Press, 3rd ed.
62. Fox RO. 2009. Optimal moment sets for multivariate direct quadrature method of moments. *Industrial & Engineering Chemistry Research* 48:9686–9696

63. Grosch R, Briesen H, Marquardt W, Wulkow M. 2007. Generalization and numerical investigation of QMOM. *AIChE Journal* 53:207–227
64. Sanyal J, Marchisio DL, Fox RO, Dhanasekharan K. 2005. On the comparison between population balance models for CFD simulation of bubble columns. *Industrial & Engineering Chemistry Research* 44:5063–5072
65. Chen P, Duduković M, Sanyal J. 2005. Three-dimensional simulation of bubble column flows with bubble coalescence and breakup. *AIChE journal* 51:696–712
66. Zucca A, Marchisio DL, Barresi AA, Fox RO. 2006. Implementation of the population balance equation in CFD codes for modelling soot formation in turbulent flames. *Chemical Engineering Science* 61:87–95
67. Bannari R, Kerdouss F, Selma B, Bannari A, Proulx P. 2008. Three-dimensional mathematical modeling of dispersed two-phase flow using class method of population balance in bubble columns. *Computers & chemical engineering* 32:3224–3237
68. Petitti M, Nasuti A, Marchisio DL, Vanni M, Baldi G, et al. 2010. Bubble size distribution modeling in stirred gas-liquid reactors with QMOM augmented by a new correction algorithm. *AIChE Journal* 56:36–53
69. Buffo A, Vanni M, Marchisio DL. 2012. Multidimensional population balance model for the simulation of turbulent gas-liquid systems in stirred tank reactors. *Chemical Engineering Science* 70:31–44
70. Buffo A, Vanni M, Marchisio D. 2017. Simulation of a reacting gas–liquid bubbly flow with CFD and PBM: Validation with experiments. *Applied Mathematical Modelling* 44:43–60
71. Li D, Gao Z, Buffo A, Podgorska W, Marchisio DL. 2017. Droplet breakage and coalescence in liquid–liquid dispersions: Comparison of different kernels with EQMOM and QMOM. *AIChE Journal* 63:2293–2311
72. Marble FE. 1970. Dynamics of dusty gases. *Annual Review of Fluid Mechanics* 2:397–446
73. Krepper E, Lucas D, Frank T, Prasser HM, Zwart PJ. 2008. The inhomogeneous MUSIG model for the simulation of polydispersed flows. *Nuclear Engineering and Design* 238:1690–1702
74. Bhole M, Joshi J, Ramkrishna D. 2008. CFD simulation of bubble columns incorporating population balance modeling. *Chemical Engineering Science* 63:2267–2282
75. Selma B, Bannari R, Proulx P. 2010. Simulation of bubbly flows: Comparison between direct quadrature method of moments (DQMOM) and method of classes (CM). *Chemical Engineering Science* 65:1925–1941
76. Silva LFLR, Lage PLC. 2011. Development and implementation of a polydispersed multiphase flow model in OpenFOAM. *Computers & Chemical Engineering* 35:2653–2666
77. Icardi M, Ronco G, Marchisio DL, Labois M. 2014. Efficient simulation of gas–liquid pipe flows using a generalized population balance equation coupled with the algebraic slip model. *Applied Mathematical Modelling* 38:4277–4290
78. Passalacqua A, Vedula P, Fox RO. 2011. Quadrature-based moment methods for polydisperse gas-solids flows. In *Computational Gas-Solids Flows and Reacting Systems: Theory, Methods and Practice*, eds. S Pannala, M Syamlal, TJ O'Brien. IGI Global, 221–244
79. Passalacqua A, Fox R, Garg R, Subramaniam S. 2010. A fully coupled quadrature-based moment method for dilute to moderately dilute fluid–particle flows. *Chemical Engineering Science* 65:2267–2283
80. Fox RO, Vedula P. 2009. Quadrature-based moment model for moderately dense polydisperse gas- particle flows. *Industrial & Engineering Chemistry Research* 49:5174–5187
81. Spalding D. 1980. Numerical computation of multi-phase fluid flow and heat transfer. In *Recent Advances in Numerical Methods in Fluids*, eds. C Taylor, K Morgan. Pineridge Press, 139–167
82. Wright Jr. DL. 2007. Numerical advection of moments of the particle size distribution in Eulerian models. *Journal of Aerosol Science* 38:352–369
83. Harten A. 1983. High resolution schemes for hyperbolic conservation laws. *Journal of computational physics* 49:357–393

84. LeVeque RJ. 2002. Finite volume methods for hyperbolic problems. Cambridge University Press, 1st ed.
85. Passalacqua A, Heylmun J, Icardi M, Bachant P, Hu X. 2018. OpenQBMM, an open-source implementation of quadrature-based moment methods. doi:10.5281/zenodo.1458280
86. Buffo A, Vanni M, Marchisio DL. 2016. On the implementation of moment transport equations in OpenFOAM: Boundedness and realizability. *International Journal of Multiphase Flow* 85:223–235
87. Pigou M, Morchain J, Fede P, Penet MI, Laronze G. 2018. New developments of the extended quadrature method of moments to solve population balance equations. *Journal of Computational Physics* 365:243–268

Table 1 Commercial and open-source CFD codes with the implementation of PBE

CFD code	Governing equation	Solution methods	Notes
OpenFOAM[a]	Equation 1 Equation 3	CM QMOM[b] CQMOM[b] EQMOM[b]	- Multi-fluid approach is available - Possibility of solving several population balances - Realizable advection schemes are implemented
Ansys Fluent	Equation 1	CM QMOM DQMOM	- Multi-fluid approach is available
Ansys CFX	Equation 1	CM	- Multi-fluid approach is available - PBE is written in terms of mass-based NDF - Continuous events and nucleation are not available
StarCCM	Equation 1	CM	- Multi-fluid approach is available - Adaptive discretization

[a]open-source; [b]as part of the OpenQBMM project (https://www.openqbmm.org) (85)

Moment Space

Any number density function $n(\xi)$ defined on a support Ω_ξ can be associated to a positive measure (μ) such that $\mathrm{d}\mu = n(\xi)\mathrm{d}\xi$. One can consider all the possible measures defined on the same support Ω_ξ, which together form a space of measures, denoted by $\mathcal{P}$. Then, each possible measure $\mu \in \mathcal{P}$ determines a possible vector of k moments (from order 0 to k): $\mathbf{m}_k = (m_0, m_1, \ldots, m_k)$. Eventually, the k^{th}-order moment space ($\mathcal{M}_k$) on the support Ω_ξ is defined as the space formed by all the possible $\mathbf{m}_k$, each corresponds to a $\mu \in \mathcal{P}$ or mathematically: $\mathcal{M}_k = \{\mathbf{m}_k = \int_{\Omega_\xi} (\xi^0, \xi^1, \ldots, \xi^k)\, \mathrm{d}\mu \quad | \quad \mu \in \mathcal{P}\}$. A set of moments $(m_0, m_1, \ldots, m_k)$ should belong to the moment space $\mathcal{M}_k$ to be realizable, otherwise no positive measure can be found with such a set of moments. The characterization of the moment space $\mathcal{M}_k$ for three common supports $\Omega_\xi = (-\infty, \infty)$, $\Omega_\xi = (0, \infty)$ and $\Omega_\xi = (0, 1)$ is found in (87).

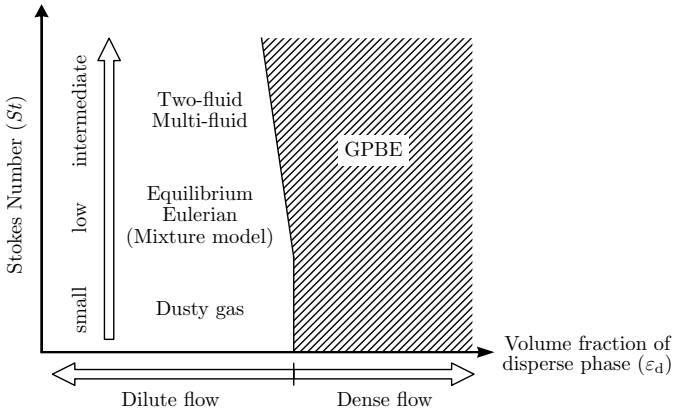

Figure 1

Applicability of the Eulerian CFD models for the simulation of multiphase flows

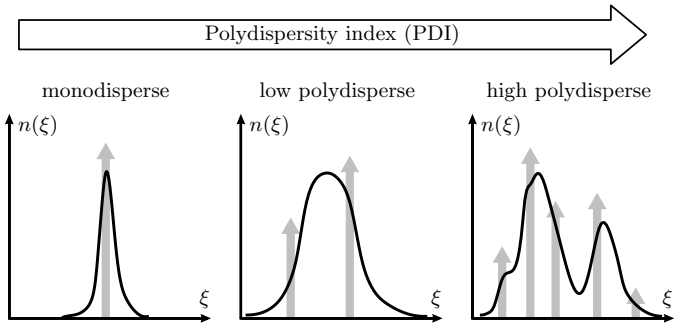

Figure 2

Polydispersity index indicates how wide is the distribution of disperse phase elements over the space of the internal coordinate. The gray arrows in above plots can be thought of as the nodes of the quadrature which approximates the underlying NDF (shown by the solid line) or as the number of element groups required to consider the polydispersity appropriately.

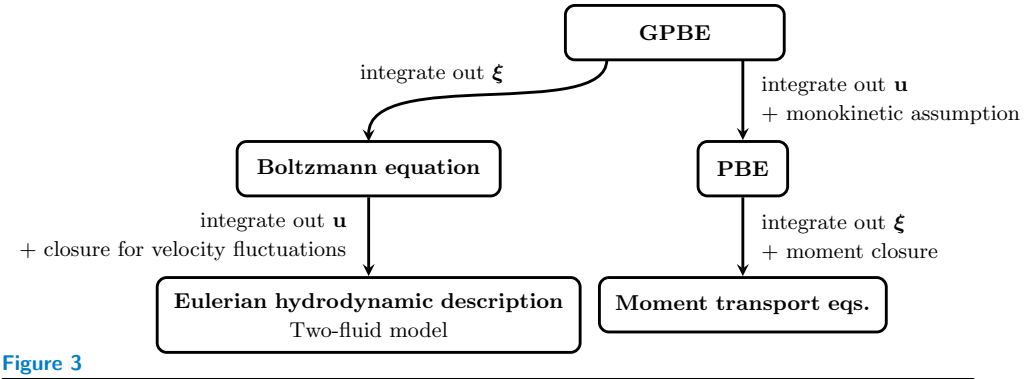

Figure 3

The relationship between the GPBE, PBE, moments and Eulerian CFD models